NleB/SseK-catalyzed arginine-glycosylation and enteropathogen virulence are finely tuned by a single variable position contiguous to the catalytic machinery

Ana García-García[1], Thomas Hicks[2], Samir El Qaidi[3], Congrui Zhu[3], Philip R. Hardwidge[3], Jesús Angulo[2,4,5*] and Ramon Hurtado-Guerrero[1,6,7*]

[1] Institute of Biocomputation and Physics of Complex Systems (BIFI), University of Zaragoza, Mariano Esquillor s/n, Campus Rio Ebro, Edificio I+D, Zaragoza, Spain.

[2] School of Pharmacy, University of East Anglia, Norwich Research Park, Norwich, NR4 7TJ, UK.

[3] College of Veterinary Medicine, Kansas State University, Manhattan, KS, 66506, USA.

[4] Departamento de Química Orgánica, Universidad de Sevilla, 41012, Sevilla, Spain.

[5] Instituto de Investigaciones Químicas (CSIC-US), 41092, Sevilla, Spain.

[6] Copenhagen Center for Glycomics, Department of Cellular and Molecular Medicine, School of Dentistry, University of Copenhagen, Copenhagen, Denmark.

[7] Fundación ARAID, Zaragoza, Spain.

*To whom correspondence should be addressed: rhurtado@bifi.es and jangulo@us.es

Supporting Methodology

Plasmid construction

The DNA sequences encoding amino acid residues of the NleB1^{EHEC} (aa 28-329), FADD death domain (DD; aa 93-192), DR3^{DD} (aa 332-417), SseK1 (aa 21-336), and SseK2 (aa 34-348) were codon optimized and synthesized by GenScript (USA) for expression in *E. coli* cells. The NleB1^{EHEC} construct also contained the K115A mutation to improve stability as described before for NleB1^{EPEC}. Lys115 is highly conserved for NleB and SseK GTs (Fig. 1a). This mutation had intact glycosyltransferase activity[1]. The wild type (wt) SseK1 and mutants contained the double mutant, C39S-C210S, which prevents protein precipitation due to irregular intermolecular disulfide binding[2]. As well as the K115A^{NleB1} mutation, the C39S-C210S^{SseK1} mutation did not affect SseK1 activity[2]. For clarification purposes, these wt-like enzymes will be named as NleB1^{EHEC} and SseK1^{wt}.

NleB1^{EHEC} and *DR3^{DD}* constructs were cloned into pMALC2x, rendering the vector pMALC2x-12Hist-TEV-*NleB1^{EHEC}* and pMALC2x-12Hist-TEV-*DR3^{DD}*, respectively. Both plasmids contained a sequence encoding a 12xHis tag and a Tobacco Etch Virus (TEV) cleavage site between the maltose binding protein (MBP) and the protein of interest. *FADD^{DD}* and *SseK1* constructs were cloned into pET15bPP, rendering the vector pET15bPP-*FADD^{DD}* and pET15bPP-*SseK1^{wt}*, respectively. Both plasmids contained a sequence encoding a 6xHis tag and a Precission Protease (PP) cleavage site located in the N-terminus of each construct. *SseK2^{wt}* construct was cloned into pProEXHTa, rendering the vector pProEXHTa-6Hist-TEV-*SseK2^{wt}*. This plasmid contained a sequence encoding a Tobacco Etch Virus (TEV) cleavage site between the 6xHis tag and the SseK2^{wt} construct. All mutants in NleB1^{EHEC}, SseK1^{wt} and SseK2^{wt} were generated following standard site-directed mutagenesis protocol by GenScript using the vectors pMALC2x-12Hist-TEV-*NleB1^{EHEC}*, pET15bPP-*SseK1^{wt}* and pProEXHTa-6Hist-TEV-*SseK2^{wt}*.

Protein expression and purification

Each plasmid was transformed into *E. coli* BL21(DE3) and grown in 2XTY medium (1.6% (w/v) tryptone, 1% (w/v) yeast extract powder and 0.5% (w/v) NaCl), containing 100 µg/ml of ampicillin at 37 ºC. When the OD_{600} reached 0.6 ~ 0.8, the culture was induced with 1 mM IPTG (isopropyl 1-thio-ß-D-galactopyranoside) at 18 ºC. After 16 h incubation, the cells were harvested by centrifugation at 10,000 rpm at 4 ºC for 10 min. Cells were lysed using buffer A (25 mM Tris pH 7.5, 500 mM NaCl, 10 mM imidazole) and loaded into a His-Trap Column (GE Healthcare). Proteins were eluted with an imidazole gradient from 10 mM to 500 mM (buffer B: 25 mM Tris pH 7.5, 500 mM NaCl, 500 mM imidazole). The buffer was exchanged to buffer C (25 mM Tris pH 7.5, 150 mM NaCl) using a HiPrep 26/10 Desalting Column (GE Healthcare) for all proteins. Thereafter, the TEV recognition site was cleaved using TEV protease for the fusion constructs containing $NleB1^{EHEC}$ and $DR3^{DD}$. TEV protease and MBP-12xHis were later removed from the solution using a His-Trap Column (GE Healthcare), and isolated $NleB1^{EHEC}$ and $DR3^{DD}$ were collected from the flow through.

The proteins were concentrated using an Amicon Ultra-15mL and quantification of proteins was carried out by absorbance at 280 nm using their theoretical extinction coefficient (the ε_{280nm} for $SseK1^{wt}$ and mutants ranged between 38,850 and 41,830 M^{-1} cm^{-1}; the ε_{280nm} for $SseK2^{wt}$ and mutants ranged between 42,350 and 44,860 M^{-1} cm^{-1}; $\varepsilon_{280nm}^{NleB1} = 55{,}810\ M^{-1}\ cm^{-1}$; $\varepsilon_{280nm}^{FADD} = 12{,}500\ M^{-1}\ cm^{-1}$; $\varepsilon_{280nm}^{DR3} = 15{,}470\ M^{-1}\ cm^{-1}$).

Isothermal titration microcalorimetry (ITC)

ITC was used to characterize the interaction of $NleB1^{EHEC}$ with UDP, $NleB1^{EHEC}$ and $S286Y^{SseK1}$ with $FADD^{DD}$ and without UDP, and $NleB1^{EHEC}$, $SseK1^{wt}$, $SseK2^{wt}$ and their corresponding mutants with $FADD^{DD}$ in the presence of an excess of UDP. All

experiments were carried out in an Auto-iTC200 (Microcal, GE Healthcare) at 25ºC. The titration of NleB1^{EHEC} with UDP was carried out at 40 μM of NleB1^{EHEC} with 500 μM of UDP in 25 mM Tris pH 7.5, 150 mM NaCl and $MnCl_2$. The titration with FADD^{DD} in the absence of UDP was determined using NleB1^{EHEC} and S286Y^{SseK1} at 40 μM and 400 μM of FADD^{DD} in 25 mM Tris pH 7.5 and 150 mM NaCl. The experiments to determine the K_ds for FADD^{DD} under an excess of UDP were made in 25 mM Tris pH 7.5, 150 mM NaCl, 1mM UDP and 0.5 mM $MnCl_2$. The concentration of NleB1^{EHEC}/SseK1^{wt}/SseK2^{wt} and their corresponding mutants were 40 μM while the FADD^{DD} concentration was ranged from 350 μM to 1 mM in the injection syringe. The experiments were performed in duplicate. Data integration, correction and analysis were carried out in Origin 7 (Microcal). The data were fit to a one-site equilibrium-binding model.

Kinetic analysis

Enzyme kinetics for the NleB1^{EHEC}, SseK1^{wt}, SseK2^{wt}, and the mutants were determined using the UDP-Glo luminescence assays (Promega). Reactions contained 10 nM of the enzymes in 25 mM Tris pH 7.5, 150 mM NaCl, 50 μM $MnCl_2$ and 500 μM UDP-GlcNAc in the presence of either FADD^{DD} or DR3^{DD}. The concentrations of FADD^{DD} and DR3^{DD} ranged from 5 to 800 μM, and from 5 to 140 μM, respectively. To determine the kinetic parameters for UDP-GlcNAc using NleB1^{EHEC}, we used 10 nM NleB1^{EHEC} in 25 mM Tris pH 7.5, 150 mM NaCl, 50 μM $MnCl_2$ and variable concentrations of UDP-GlcNAc (from 5 to 800 μM) in the presence of the 800 μM FADD^{DD}. Reactions were incubated 30 minutes at 30ºC and stopped using 5 μl of UDP-detection reagent at a 1:1 ratio in a white and opaque 384-well plate. Then, the plates were incubated in the dark for 1 h at room temperature. Subsequently, the values were obtained by using a Synergy HT (Biotek).

To estimate the amount of UDP produced in the glycosyltransferase reaction, we created a UDP standard curve. The values were corrected against the UDP-GlcNAc hydrolysis and were fit to a non-linear Michaelis-Menten or Michaelis-Menten with substrate inhibition programs in GraphPad Prism 6 software from which the K_m, k_{cat}, V_{max} and K_i along with their standard deviations were obtained. All experiments were performed in duplicate.

Salmonella infection of macrophages

Macrophage infection assays were performed to measure the intracellular abundance of complemented *Salmonella* Δ*sseK1*Δ*sseK2*Δ*sseK3* strains[3] in RAW264.7 cells. RAW264.7 cells were seeded at 1 x 10^5 cells/well in 24-well plates 24 h before infection. Bacterial cultures were grown to an OD_{600} of 0.4 and 10^6 CFUs were added to RAW264.7 cells for 30 min. Cells were then incubated in medium containing 100 µg/mL gentamicin for 1 h, and then 10 µg/mL gentamicin for an additional 23 h. Bacteria were released from RAW264.7 cells using 1% saponin, diluted in PBS, and plated for colony counts.

Molecular dynamics (MD) simulations

The starting complexes were prepared using Schrödinger Maestro. Cartesian co-ordinates for the NleB1^{EPEC}-UDP-Mn^{+2}-FADD^{DD} complex[1] were taken from the protein data bank (PDB entry 6ACI). The UDP-GlcNAc was added manually but based on the UDP coordinates of the above complex. The system was then prepared using the protein preparation wizard[4]. Hydrogen atoms were all added and the ionisation state of side chains was predicted with PROPKA[5]. The resulting structure was minimised with OPLS[6] using a threshold of 0.3 Å to converge heavy atoms.

The Cartesian coordinates of the enzyme were taken from the crystal structure of SseK1^{wt} (PDB entry 5H60)[2], from which all the three single mutants were built (S286Y^{SseK1}, S286N^{SseK1} and S286I^{SseK1}). Missing lid domain residues were first added using the build tool and numbered appropriately. The system was then prepared using the protein preparation wizard[4]. Hydrogen atoms were all added and any ligands and non-structurally important waters were removed. The ionization state of side chains was predicted with PROPKA[5]. The resulting structure was minimised with OPLS[6] using a threshold of 0.3 Å to converge heavy atoms. For each complex, UDP-GlcNAc was docked into the donor site and their complexes with the acceptor, FADD^{DD}, were constructed by structural alignment of the enzyme with NleB1^{EPEC} in the crystal structure of the NleB1^{EPEC}-UDP-Mn^{+2}-FADD complex[1] followed by energy optimization. UDP-GlcNAc was prepared in Maestro using LigPrep with a series of low-energy conformations generated by MacroModel. The conformers were then docked into a grid with outer box dimensions of 23 Å x 23 Å x 23 Å and inner box dimensions of 10 Å x 10 Å x 10 Å with the centroid of the box placed in the middle of the UDP-GlcNAc binding site. UDP-GlcNAc was then docked using Glide[7, 8] with standard precision and a 2-times sampling without ring canonicalization and sampling ring conformations. One resulting structure was selected from the docking and used to build all of the complexes of SseK1 and mutants.

The MD simulations charges for the UDP fragment of UDP-GlcNAc were derived from the RESP fitting method[9] and with the overall charge set to -2. To be compatible with GLYCAM[10] the charges for this fragment were calculated with the GlcNAc ring substituted with a methyl group. The methyl group was given a charge of 0.194 prior to removal leaving a total charge of -2.194 for the methylated UDP fragment.

Molecular dynamics simulations of the NleB1^{EPEC}-UDP-GlcNAc-Mn^{+2}-FADD, SseK1^{wt}-UDP-GlcNAc-Mn^{+2}-FADD, and S286Y/N/I-UDP-GlcNAc-Mn^{+2}-FADD complexes

were performed using Amber PMEMD[11]. The Amber *ff11SB* force field was used to parameterise all protein atoms with the Mn^{2+} ion modelled using a 12-6-4 LJ-type parameters derived from *Amber ions234lm_1264_tip3p*. GLYCAM 06j and GAFF was used to parameterise the sugar nucleotide, UDP-GlcNAc. All of the systems were solvated using a truncated octahedral box using TIP3P water with a buffer set to 10 Å. The system was neutralised using Na^+ ions. The conjugate gradient algorithm was used to minimise the systems with convergence threshold set to 10^{-4} kcal mol^{-1} $Å^{-1}$, first using a 20 kcal mol^{-1} $Å^{-2}$ restrain on solute atoms after which minimisation was repeated without any restraints. Each system was then heated to a temperature of 310 K over 500 ps prior to pressure equilibration to 1 atm over the course of another 500 ps. During both heating and pressure equilibration restraints of 20 kcal mol^{-1} A^{-2} were placed on solute atoms. Restraints were then released from the system in four stages, each of 200 ps length. Then, Gaussian accelerated Molecular Dynamics (GaMD) was used to simulate each system for 1 μs. GaMD was used as implemented in Amber with the use of boost potentials on dihedrals and total potential energy. In this the simulations are each broken into four stages. The first stage is a standard 2 ns MD simulation in order calculate the boost potential. This boost potential is then used to simulate the first 400 ps of the simulation prior to allowing for adaptation for 5.6 ns. The final boost potential was then used to perform the molecular dynamics simulation for 1 μs with co-ordinates being saved every 100 ps. The SHAKE algorithm was used in all simulations to restrain bonds to hydrogen atoms, with the time step being set to 2 fs. To maintain temperature a Langevin thermostat was implemented using a collision frequency of 5 ps^{-1}. To maintain pressure an isotropic Berendsen algorithm was used as a barostat with relaxation time set to 1 ps. Periodic boundary conditions were used with particle mesh Ewald for calculating electrostatics.

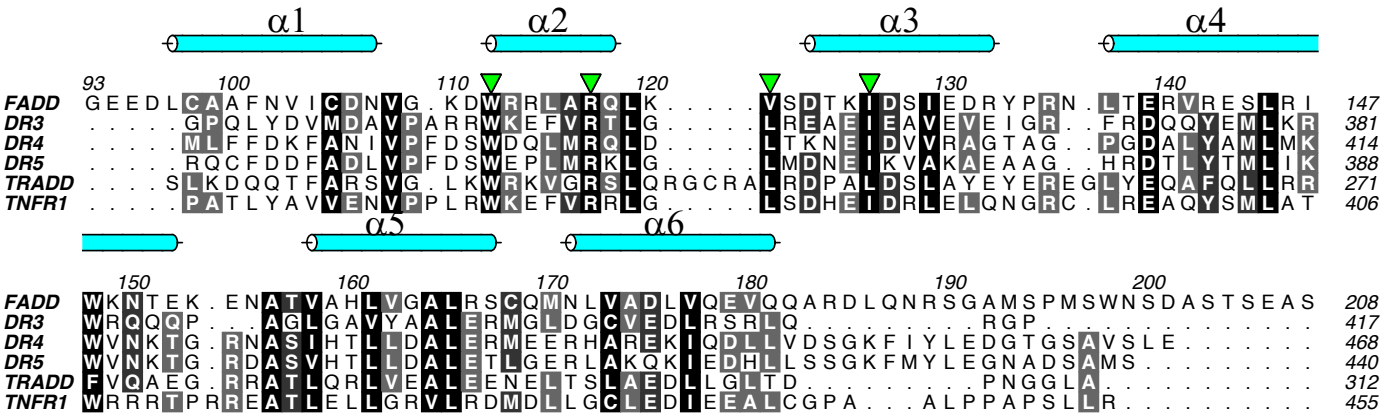

Fig. S1. Multiple sequence alignment of death domains-containing proteins. For practical purposes, only the DDs are shown in the alignment. Note that NleB1^{EPEC} cannot glycosylate TNF-associated apoptosis-inducing ligand (TRAIL) receptor 1 (TRAIL-R1, also known as DR4), and TRAIL-R2 (DR5)[1]. The residues indicated by inverted green triangles are highly conserved within these domains and are also engaged in interactions with NleB1^{EPEC}. α-helices are shown for FADD within the NleB1^{EPEC}-UDP-Mn^{+2}-FADD^{DD} complex[1].

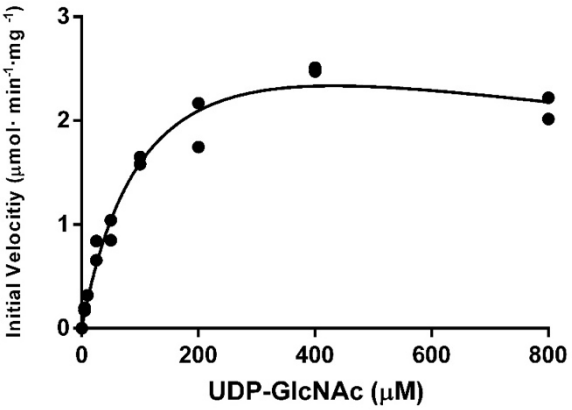

Fig. S2. Kinetics of NleB1^{EHEC} against variable concentrations of UDP-GlcNAc using 800 μM FADD^{DD}.

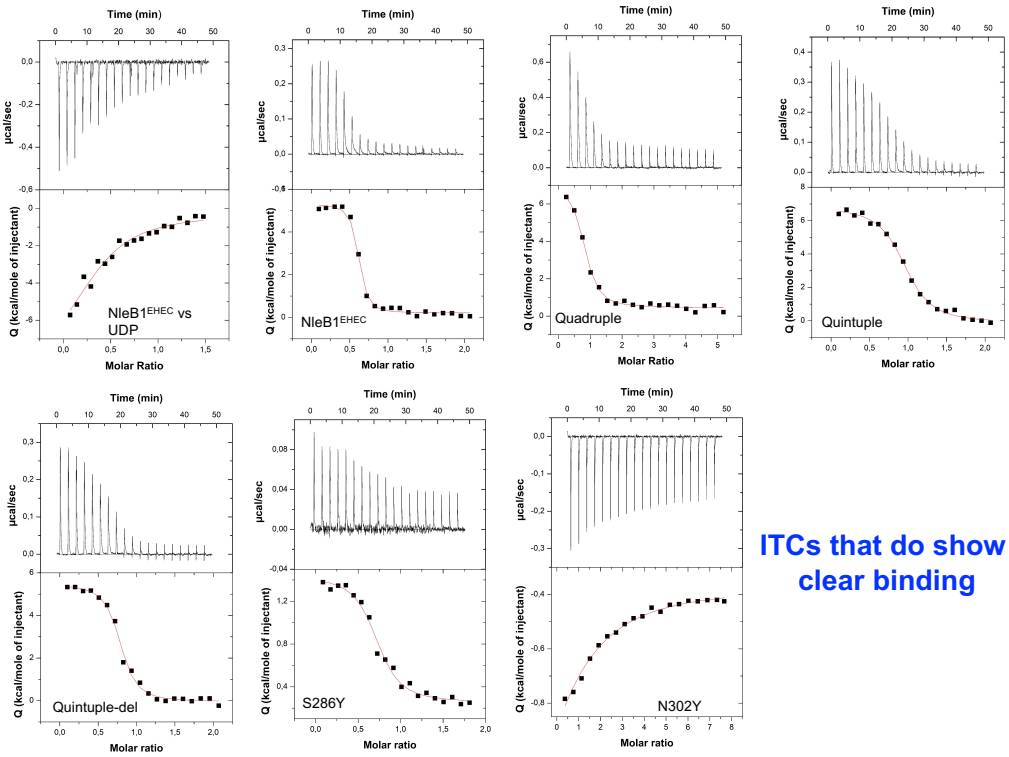

ITCs that do show clear binding

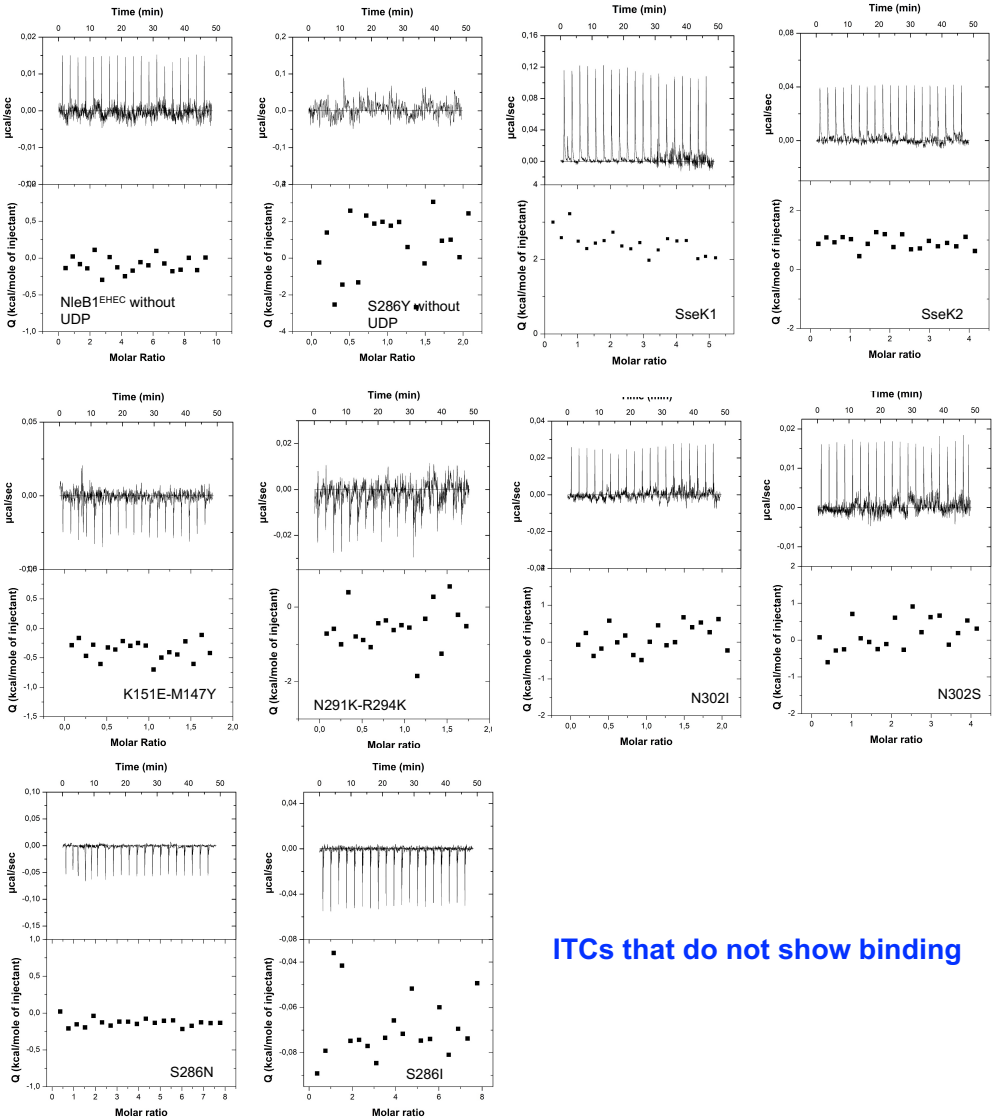

ITCs that do not show binding

Fig. S3. ITC data for the binding of $FADD^{DD}$ to $NleB1^{EHEC}$, $SseK1^{wt}$, $SseK2^{wt}$ and the SseK1/SseK2 mutants. Top: raw thermogram (thermal power versus time). Bottom: binding isotherm (normalized heats versus molar ratio). Except for the ITC experiment in which the K_d was determined for UDP in the presence of $NleB1^{EHEC}$ and $MnCl_2$ (text highlighted in blue), the rest of the ITCs were performed in the presence of FADD either in the absence or presence of UDP. See Table S3 for the thermodynamic and K_d values for all the experiments.

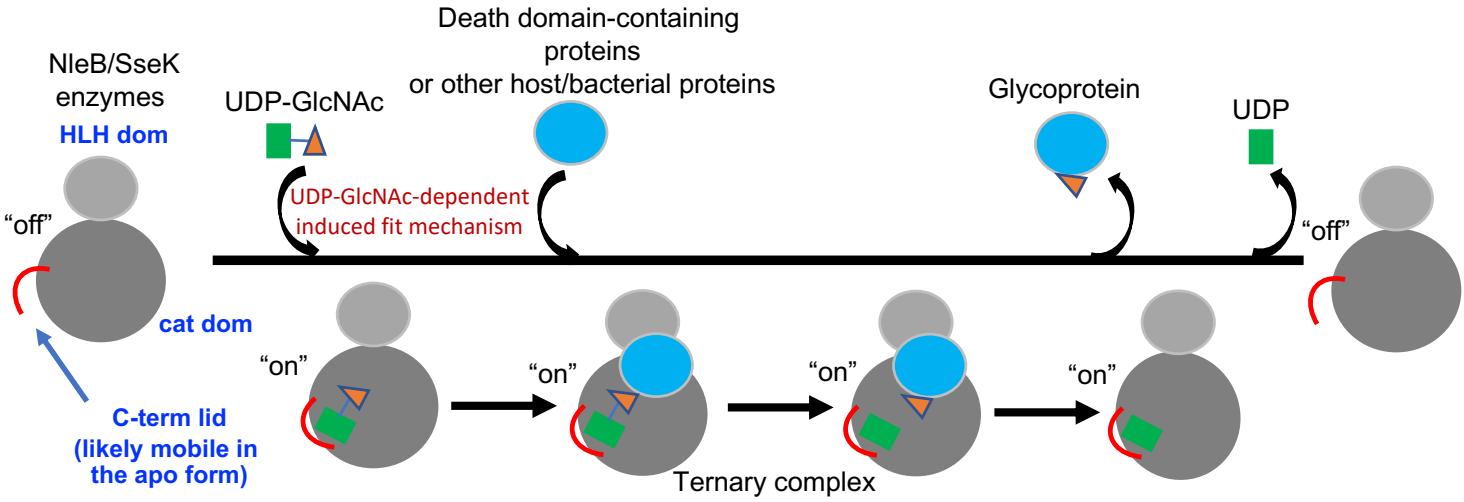

Fig. S4. Dynamics of NleB/SseK GTs along the catalytic cycle. The scheme shows an ordered kinetic mechanism for these enzymes in which UDP-GlcNAc induces a fit mechanism to close the C-terminal lid and generate the active form of these enzymes. In the apo-form, the lid is flexible and likely open, and the enzymes are in an inactive form. As we previously reported[2], the C-terminal lid in the SseK2^{wt} apo form is disordered and gets ordered in the presence of UDP or UDP-GlcNAc/$MnCl_2$. Only after these enzymes are in the active state, the DD-containing proteins or other bacterial/host proteins can bind, and the catalysis can take place. Note that in the NleB1^{EPEC}-UDP-FADD^{DD} complex[1], no interactions were observed between the C-terminal lid residues and FADD^{DD}. However, the closure of the C-terminal lid is a prior requisite for an optimal binding to the protein substrate. Note that the binding to UDP-GlcNAc needs the presence of Mn^{+2} although this is not indicated in the scheme.

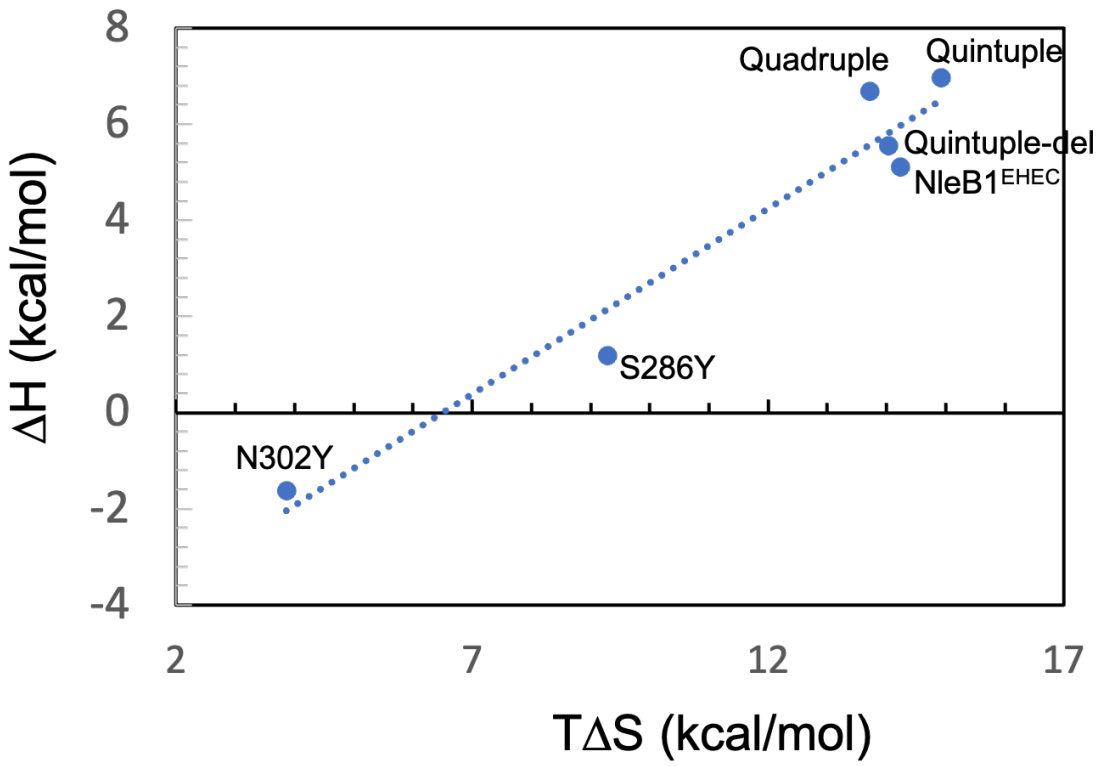

Fig. S5. Thermodynamics parameters (ΔH and TΔS) from ITC for the binding of FADD with NleB1 and different single or multiple mutants. The dashed line indicates good correlation with an enthalpy-entropy compensation behavior, where multiple mutants show similar thermodynamic profiles to that of NleB1, whereas single mutants $S286Y^{SseK1}$ and $N302Y^{SseK2}$ benefit from enthalpy, with less favorable entropy components.

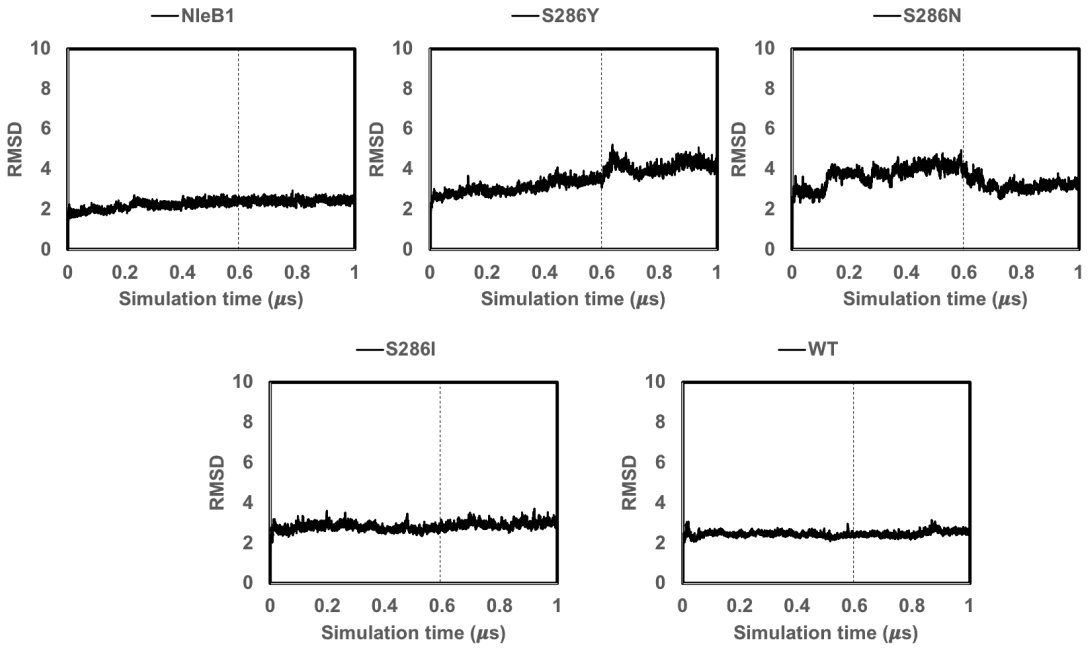

Fig. S6. Molecular dynamics of the complexes of $FADD^{DD}$ with $NleB1^{EPEC}$, $S286Y^{SseK1}$, $S286N^{SseK1}$, $S286I^{SseK1}$ and $SseK1^{wt}$. Root mean square deviations (Å) of the backbone atoms of the five complexes along the 1 μs trajectory. All showed stability along the entire simulation time, indicating that the simulation length, although suitable to sample processes in the time scale of internal structural dynamics, is not long enough to simulate dissociation from the bound state for those complexes with the lowest affinities. Thus, the complex of $FADD^{DD}$ with $S286N^{SseK1}$, which shows poor glycosylation activity, as well as those of $FADD^{DD}$ with $SseK1^{wt}$ and $S286I^{SseK1}$, which are inactive, are likely to have poor affinity, yet these complexes are stable in such a simulation time. This allows us to monitor the differential behavior of the 5 complexes around the point of mutation along the GaMD simulations. The dynamics of the HLH motif on the single mutant $S286Y^{SseK1}$ vertical produced an increase in the RMSD values up to around 0.6 μs. The vertical dotted line indicates the time from which the structural analysis of the complexes was carried out after all the complexes reached the steady limit.

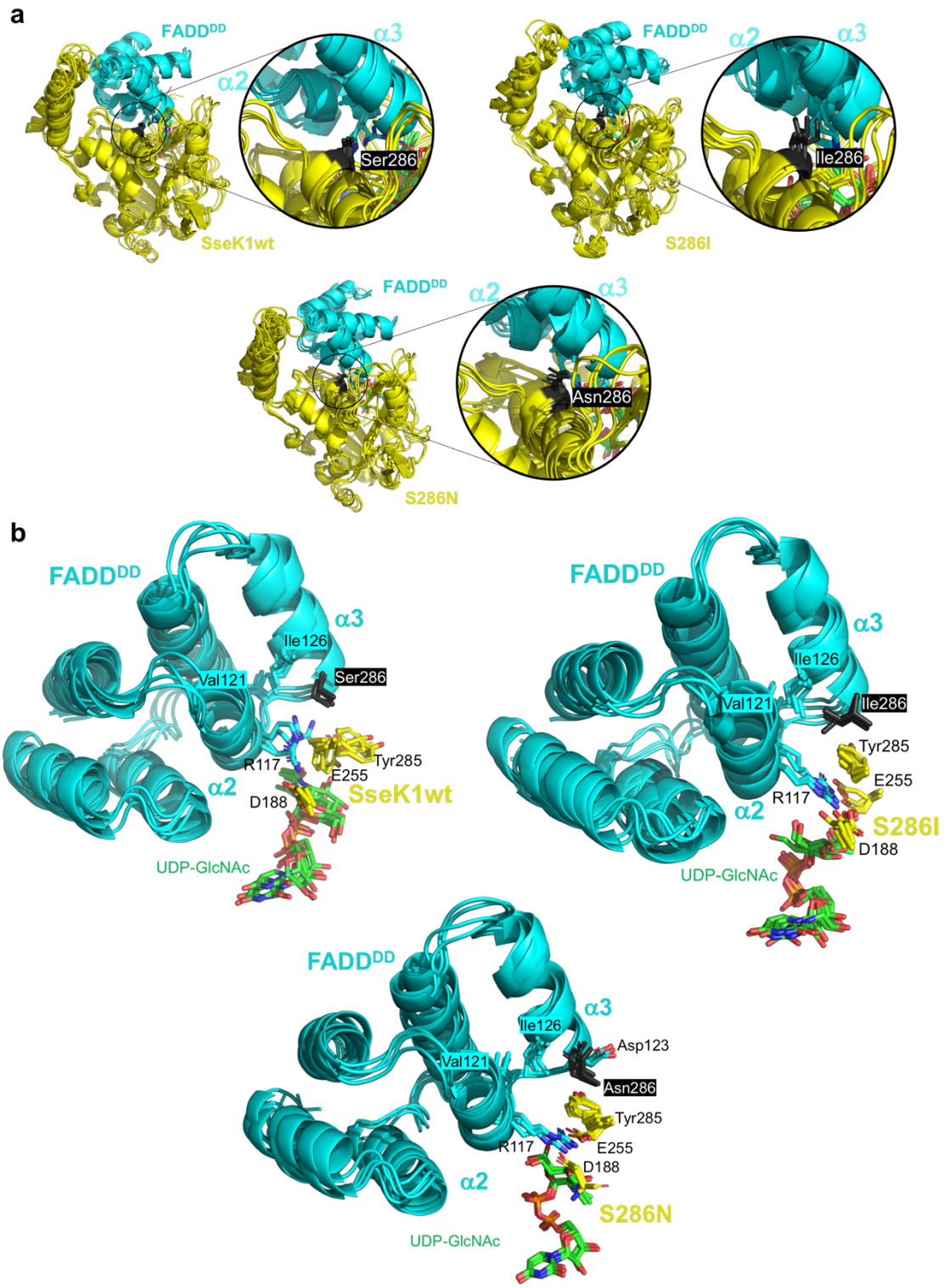

Fig. S7. Molecular dynamics of the complexes of $FADD^{DD}$ with $SseK1^{wt}$, $S286I^{SseK1}$ and $S286N^{SseK1}$. Superposition of MD frames (0.7, 0.8, 0.9 and 1.0 μs) of the complexes. (A) Proteins are in cartoon representation (enzyme in yellow, acceptor $FADD^{DD}$ in cyan), and the side chain at the point of mutation ($Ser286^{SseK1}$, $Ile286^{SseK1}$ or $Asn286^{SseK1}$) is in black

sticks. (B) Expansions of the key residues at the interface of contact involving the catalytic domain ($FADD^{DD}$ in cyan cartoon representation; $Ser286^{SseK1}$, $Ile286^{SseK1}$ or $Asn286^{SseK1}$ in black sticks; key $SseK1^{wt}$, $S286I^{SseK1}$, or $S286N^{SseK1}$ residues in yellow sticks). In the case of the $S286N^{SseK1}$ mutant, the $FADD^{DD}$ residue $Asp123^{FADD}$ is represented in sticks as it makes favorable contacts with the side chain of $Asn286^{SseK1}$. The side chains of $Ser286^{SseK1}$ in the $SseK1^{wt}$ and $Asn286^{SseK1}$ in the $S286N^{SseK1}$ mutant, are too small as to establish favorable contacts with $Val121^{FADD}$ and $Ile126^{FADD}$ in the groove between α2 and α3 helices. On the contrary, the side chain of $Ile286^{SseK1}$ in the $S286I^{SseK1}$ mutant is too bulky and cannot enter the groove, also lacking those favorable contacts (cf. Fig. 3 in the main text).

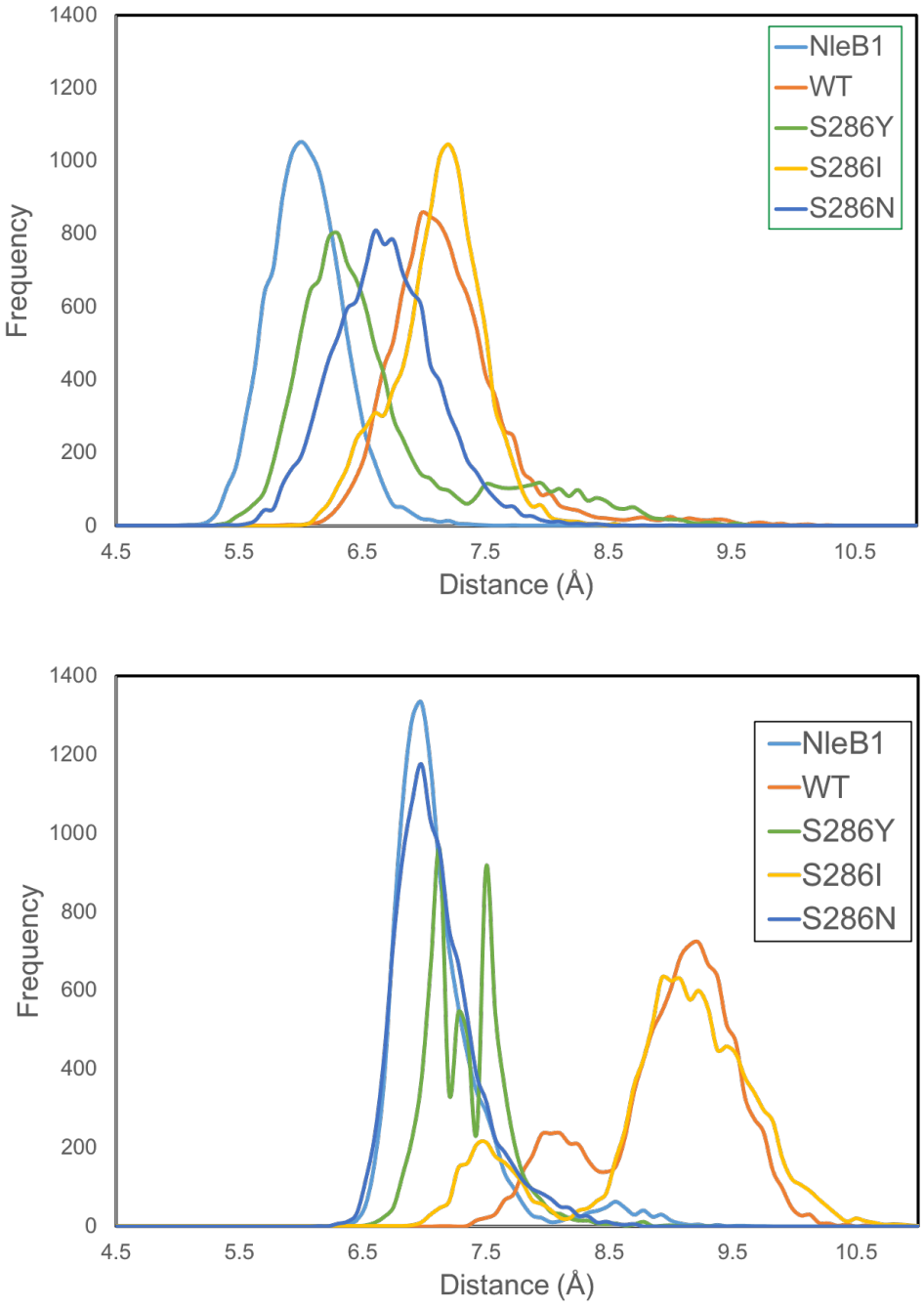

Fig. S8. Distributions of key intermolecular distances of the complexes of $FADD^{DD}$ with $NleB1^{EPEC}$, $SseK1^{wt}$, $S286Y^{SseK1}$, $S286I^{SseK1}$ and $S286N^{SseK1}$. (top) Distances from the center of mass of the side chain of $Ile126^{FADD}$ to the center of mass of the side chain of the amino acid residue at the point of mutation (i.e. $Tyr284^{NleB1}$ (light blue), $Ser286^{SseK1}$ (red), $Tyr286^{S286Y}$ (green), $Ile286^{S286I}$ (yellow), $Asn286^{S286N}$ (dark blue)). $Tyr286^{S286Y}$ in the $S286Y^{SseK1}$ mutant shows good contacts along the MD simulation with the side chain

of Ile126^{FADD}, approaching the behavior of NleB1^{EPEC}. Ser286^{SseK1} and Ile286^{S286I} do not make contacts with Ile126^{FADD}, due to the small and large size of their side chain, respectively. Asn286^{S286N} gets closer to the side chain of Ile126^{FADD} at certain stages of the MD simulation. (bottom) Distances from the central guanidinium carbon of Arg117^{FADD} to the central carboxylic carbon of either Asp186^{NleB1} (light blue), Asp188^{SseK1} (red), Asp188^{S286Y} (green), Asp188^{S286I} (yellow), or Asp188^{S286N} (dark blue). The shortest distances correlate with the presence of stable H-bond interactions along the MD simulations between the side chain of Arg117^{FADD} with the carboxylate side chains of Asp186^{NleB1}, Asp188^{S286Y}, and Asp188^{S286N}.

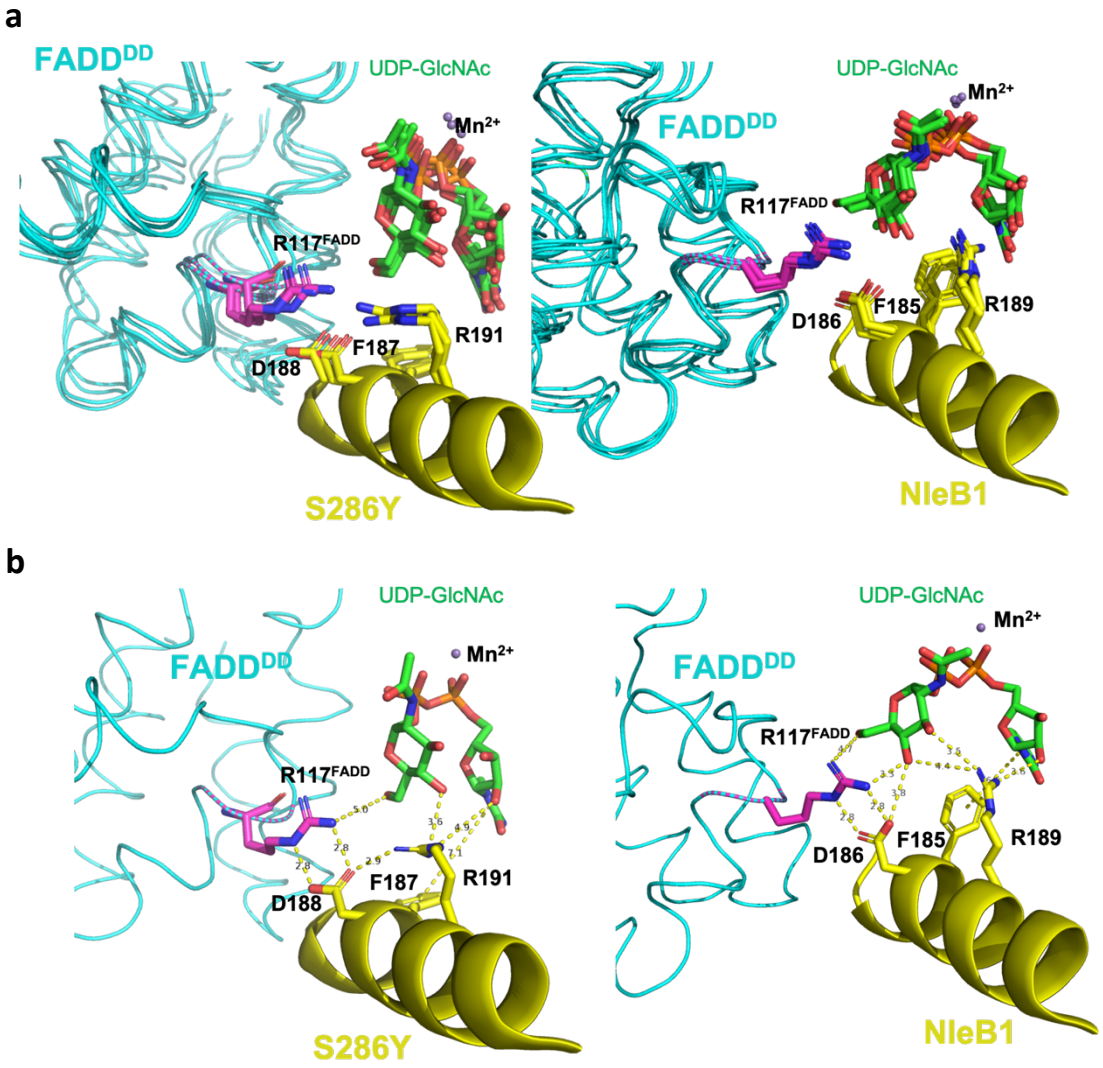

Fig. S9. Molecular dynamics of the complexes of $FADD^{DD}$ with $S286Y^{SseK1}$ and NleB1 in the presence of the donor substrate UDP-GlcNAc and Mn^{2+}. The interactions of the Asp/Arg dyad (D188/R191 in S286Y, and D186/R189 in NleB1), explain the requirement of the presence of the bound sugar nucleotide for $FADD^{DD}$ binding to occur (ordered bi-bi mechanism) (A) Superposition of MD frames (0.7, 0.8, 0.9 and 1.0 μs) of the complexes of $S286Y^{SseK1}$ (left) and NleB1 (right) with $FADD^{DD}$. (B) Networks of interactions highlighted for one frame of the simulation (1.0 μs) for both complexes.

Table S1. Table of interactions between NleB1^{EPEC}-FADD interface residues. The residues highlighted in bold were targeted for site-directed mutagenesis for the corresponding aligned residues of SseK1^{wt} and SseK2^{wt}.

Amino acid (NleB1^{EPEC})	Amino acid (FADD^{DD})	Type of interaction	Degree of conservation with SseKs
Y145 (side chain)	R135 (side chain)	CH-π	Non-conserved
E149 (backbone)	R135 (side chain)	Hydrogen bond	Non-conserved with SseK1^{wt} and SseK3^{wt}
D151 (side chain)	L137 (backbone)	Hydrogen bond	Conserved
Y153 (side chain)	L137 (side chain)	CH-CH	Conserved (at the level of hydrophobicity)
L154 (side chain)	L137 (side chain)	CH-CH	Conserved
E253 (side chain)	R117 (side chain)	Salt bridge	Conserved
K277 (side chain)	E130 (side chain)	Salt bridge	Conserved
D279 (side chain) D279 (side chain)	R113 (side chain) W112 (side chain)	Salt bridge Hydrogen bond	Conserved with SseK1^{wt}
Y283 (side chain)	R117 (side chain)	Cation-π	Conserved
Y284 (side chain) **Y284** (side chain)	V121 (backbone) I126 (side chain)	Hydrogen bond CH-π	Non-conserved
D285 (side chain)	R113 (side chain)	Salt bridge	Conserved
K289 (side chain)	E130 (side chain)	Salt bridge	Non-conserved with SseK1^{wt} and SseK3^{wt}
K292 (side chain)	D123 (side chain)	Salt bridge	Partly conserved (Arg residue in all SseK GTs)
Y303 (side chain)	D123 (side chain)	Hydrogen bond	Conserved

Table S2. Kinetic parameters of the $FADD^{DD}$ used in this study using the $NleB1^{EHEC}$, $SseK1^{wt}$, $SseK2^{wt}$ and the SseK1/SseK2 mutants. Note that the first row defines the kinetic parameters for UDP-GlcNAc using the $NleB1^{EHEC}$ (text highlighted in bold). $NleB1^{EHEC}$ was the only enzyme showing substrate inhibition under the presence of variable concentrations of $FADD^{DD}$.

	K_m (μM)	R^2	V_{max} (μmol·min^{-1}·mg^{-1})	k_{cat} (min^{-1})	k_{cat}/K_m (min^{-1}·μM^{-1})	K_i (μM)
$NleB1^{EHEC}$ (UDP-GlcNAc)	**125 ± 33**	**0.98**	**2.5 ± 0.22**	**94 ± 8.1**	**0.75**	**-**
$NleB1^{EHEC}$	13 ± 2.5	0.94	2.92± 0.20	107 ± 7.6	8.2	793 ± 160
$SseK1^{wt}$	***	***	***	***	***	-
Quintuple-del	27 ± 4.7	0.97	1.35 ± 0.14	49 ± 5.2	1.8	-
S286Y	57 ± 12.0	0.95	1.86 ± 0.10	68 ± 3.9	1.2	-
Quintuple	31 ± 2.8	0.99	1.23 ± 0.04	45 ± 1.6	1.45	-
Quadruple	79 ± 36.7	0.90	0.67 ± 0.21	25 ± 7.8	0.3	-
K151E-M147Y	**	**	**	**	**	-
N291K-R294K	**	**	**	**	**	-
S286I	***	***	***	***	***	-
S286N	**	**	**	**	**	-
$SseK2^{wt}$*	1,226 ± 574	0.96	0.43 ± 0.13	16 ± 4.9	0.013	-
N302Y	157 ± 28.3	0.96	1.8 ± 0.13	64 ± 4.7	0.41	-
N302I	***	***	***	***	***	-
N302S	***	***	***	***	***	-

*The kinetic parameters for $SseK2^{wt}$ are not reliable because all the kinetic parameters are estimated. Note that the software estimates a K_m of 1226 μM when the maximum concentration of $FADD^{DD}$ in the experiment is 800 μM.
**Not determined (data could not be fitted to the non-linear Michaelis-Menten equation because under our conditions, these mutants showed a linear increase on the activity versus the variable concentrations of $FADD^{DD}$).
***Not active.

Table S3. Thermodynamic parameters for $FADD^{DD}$ binding to $NleB1^{EHEC}$, $SseK1^{wt}$, $SseK2^{wt}$ and the SseK1/SseK2 mutants. K_d is the dissociation constant (=1/K), and ΔG, ΔH and -TΔS are the thermodynamic parameters. Stoichiometry of binding in all cases was close to ~1:1. Except for the first ITC experiment in which the K_d was determined for UDP in the presence of $NleB1^{EHEC}$ and $MnCl_2$ (text highlighted in bold), the rest of the ITCs were performed in the presence of FADD either in the absence or presence of UDP.

	K_d (μM)	ΔG (Kcal/mol)	ΔH (Kcal/mol)	-TΔS (Kcal/mol)	N
$NleB1^{EHEC}$ (UDP)	**14.92 ± 1.11**	**-6.05 ± 0.45**	**-8.45 ± -3.4**	**2.4 ± 0.96**	**0.60**
$NleB1^{EHEC}$	0.2 ± 0.04	-9.1 ± 1.82	5.12 ± 0.11	-14.22 ± 2.84	0.67
$NleB1^{EHEC}$ (without UDP)	*	*	*	*	*
$SseK1^{wt}$	*	*	*	*	*
Quintuple-del	0.58 ± 0.12	-8.48 ± 1.75	5.56 ± 0.15	-14.03 ± 2.98	0.76
S286Y	1.11 ± 0.31	-8.09 ± 2.26	1.19 ± 0.02	-9.28 ± 2.59	0.7
S286Y (without UDP)	*	*	*	*	*
Quintuple	1.28 ± 0.18	-8.01 ± 1.12	6.98 ± 0.01	-14.92 ± 2.09	0.94
Quadruple	2.55 ± 0.5	-7.02 ± 1.38	6.69 ± 0.3	-13.71 ± 2.7	0.75
K151E-M147Y	*	*	*	*	*
N291K-R294K	*	*	*	*	*
S286I	*	*	*	*	*
S286N	*	*	*	*	*
SseK2	*	*	*	*	*
N302Y	94.4 ± 21.9	-5.47 ± 1.27	-1.61 ± 0.16	-3.86 ± 0.89	0.98
N302I	*	*	*	*	*
N302S	*	*	*	*	*

*Not measurable under our conditions. This might be due that the binding is very weak. Besides, we could not increase the concentration of $FADD^{DD}$ over 1 mM due to solubility issues. Therefore, we could not observe titration with any of these mutants against $FADD^{DD}$.

Table S4. Root mean square fluctuations from the 1 μs GaMD simulations of the five complexes.

	RMSF (Å)
$NleB1^{EPEC}$:FADD	0.71
$SseK1^{wt}$:FADD	1.27
$S286Y^{SseK1}$:FADD	0.95
$S286I^{SseK1}$:FADD	1.00
$S286N^{SseK1}$:FADD	0.80

Table S5. Kinetic parameters of the $DR3^{DD}$ used in this study using the $NleB1^{EHEC}$, $SseK1^{wt}$, $SseK2^{wt}$ and the SseK1/SseK2 mutants.

	K_m (μM)	R^2	V_{max} (μmol·min^{-1}·mg^{-1})	k_{cat} (min^{-1})	k_{cat}/K_m (min^{-1}·μM^{-1})
$NleB1^{EHEC}$	50.5 ± 9.05	0.979	2.5 ± 0.18	87.1 ± 6.3	1.72
$SseK1^{wt}$	125 ± 25.75	0.994	1.1 ± 0.13	40 ± 4.4	0.32
$S286Y^{wt}$	45 ± 8.7	0.972	1.3 ± 0.1	47 ± 3.5	1.04
S286I	**	**	**	**	**
S286N	***	***	***	***	***
SseK2	***	***	***	***	***
N302Y*	166 ± 18.5	0.997	2.0 ± 0.14	70 ± 5	0.42
N302I	**	**	**	**	**
N302S	**	**	**	**	**

The kinetic parameters for N302Y are not reliable because all the kinetic parameters are estimated. Note that the software estimates a K_m of 166 μM when the maximum concentration of $DR3^{DD}$ in the experiment is 140 μM.
**Not determined (data could not be fitted to the non-linear Michaelis-Menten equation because under our conditions, these mutants showed a linear increase on the activity versus the variable concentrations of $FADD^{DD}$). Besides, we could not use higher concentrations of $DR3^{DD}$ because of solubility issues.
***Not active

REFERENCES

1. J. Ding, X. Pan, L. Du, Q. Yao, J. Xue, H. Yao, D. C. Wang, S. Li and F. Shao, *Mol Cell*, 2019, **74**, 922-935 e926.
2. J. B. Park, Y. H. Kim, Y. Yoo, J. Kim, S. H. Jun, J. W. Cho, S. El Qaidi, S. Walpole, S. Monaco, A. A. Garcia-Garcia, M. Wu, M. P. Hays, R. Hurtado-Guerrero, J. Angulo, P. R. Hardwidge, J. S. Shin and H. S. Cho, *Nat Commun*, 2018, **9**, 4283.
3. S. El Qaidi, C. Zhu, P. McDonald, A. Roy, P. K. Maity, D. Rane, C. Perera and P. R. Hardwidge, *Front Cell Infect Microbiol*, 2018, **8**, 435.
4. G. M. Sastry, M. Adzhigirey, T. Day, R. Annabhimoju and W. Sherman, *J Comput Aided Mol Des*, 2013, **27**, 221-234.
5. M. H. Olsson, C. R. Sondergaard, M. Rostkowski and J. H. Jensen, *J Chem Theory Comput*, 2011, **7**, 525-537.
6. E. Harder, W. Damm, J. Maple, C. Wu, M. Reboul, J. Y. Xiang, L. Wang, D. Lupyan, M. K. Dahlgren, J. L. Knight, J. W. Kaus, D. S. Cerutti, G. Krilov, W. L. Jorgensen, R. Abel and R. A. Friesner, *J Chem Theory Comput*, 2016, **12**, 281-296.
7. T. A. Halgren, R. B. Murphy, R. A. Friesner, H. S. Beard, L. L. Frye, W. T. Pollard and J. L. Banks, *J Med Chem*, 2004, **47**, 1750-1759.
8. R. A. Friesner, J. L. Banks, R. B. Murphy, T. A. Halgren, J. J. Klicic, D. T. Mainz, M. P. Repasky, E. H. Knoll, M. Shelley, J. K. Perry, D. E. Shaw, P. Francis and P. S. Shenkin, *J Med Chem*, 2004, **47**, 1739-1749.
9. E. Vanquelef, S. Simon, G. Marquant, E. Garcia, G. Klimerak, J. C. Delepine, P. Cieplak and F. Y. Dupradeau, *Nucleic Acids Res*, 2011, **39**, W511-517.
10. K. N. Kirschner, A. B. Yongye, S. M. Tschampel, J. Gonzalez-Outeirino, C. R. Daniels, B. L. Foley and R. J. Woods, *J Comput Chem*, 2008, **29**, 622-655.
11. R. Salomon-Ferrer, A. W. Gotz, D. Poole, S. Le Grand and R. C. Walker, *J Chem Theory Comput*, 2013, **9**, 3878-3888.